Lead-tungstate crystals for a high performance electromagnetic calorimeter

Ryota Kohara
M1379013
Department of Physical Science
Hiroshima University Graduate School of Science

February 10, 2002

Abstract

A large amount of particles is produced in ultra relativistic heavy ion collisions (Au−Au or Pb−Pb) compared with elementary reactions (e^+e^- or $p\bar{p}$) in a unit solid angle. We need the electromagnetic calorimeter with high granularity in order to measure electromagnetic particles accurately in such a high partiecle multiplicity environment. It is essential to develop calorimeter materials as scintillators with the small Molière radius because the position resolution strongly depends on the Molière radius as long as we fix the total volume of the calorimeter. We also request the calorimeter with high energy resolution to efficiently identify a particle which decayed into electromagnetic particles. It is important to increase the amount of scintillation light and to improve its uniformity and transparency because the energy resolution relys on these characteristics. The high resolution calorimeter would drastically enhance the discovery potential for photons directly emitted from a hot and dense matter created in heavy ion collisions. We made lead tungstate ($PbWO_4$ or PWO) crystals doped yttrium at Furukawa Co., Japan. We consider PWO crystals to be the best candidate for a high performance electromagnetic calorimeter because of its smallest Molière radius of 2.2 [cm] in the inorganic scintillators. We have Y-doped PWO crystals with the dimensions of $20\times20\times200$ [mm^3]. The size is adequate for real applications.

We tested two PWO samples coupled with photomultipliers irradiated by $\gamma-$rays from a ^{60}Co source for measurements of scitillation properties at room temperature. The light yields were found to be 4.5 and 8.2 photoelectrons per deposit energy in unit of MeV ([p.e./MeV]). The decay time spectums of light emission were expressed by fast and slow compents of 1.7 [ns] (30%) and 5.6 [ns] (70%), 1.2 [ns] (17%) and 6.0 [ns] (83%), respectively. We also observed the difference of the light yield between the two crystals by cosmic particles passing though the crystal, even though they were manufactured with the same method. The PWO crystals have the small light output but very fast response of scintillation in comparision of a bismuth germanate (BGO) crystal, same size as our PWO samples, whose light yield was 404 [p.e./MeV] and decay time was 185 [ns]. At REFER and KEK−PS, an electron beam of 150 [MeV] and hadron beam of 1 to 3 [GeV] impinged on the single PWO crystal longitudinally. We found that in the single crystal the average of the energy containment was 78 % for these energies, and the energy resolution was $5.6\%/\sqrt{E}$ (where E is the incident electron or positorn energy in unit of GeV). We simulated the electromagnetic shower initiated by incident electrons with the GEANT4 code. The simulated results are consisted with the experimental beam test in the single crystal on the stochastic term ,taken into account the statistics of the scintillation light. We concluded that the energy resolution will be up to $1.8\%/\sqrt{E}$ with nine crystals arranged in a 3×3 matrix.

Contents

List of Figures

List of Tables

Chapter 1

Introduction

Quantum chromodynamics (QCD), the theory of strong interactions, with statistical treatment predicts the phase transition from a confined state of quarks and gluons as normal nuclear matter into a deconfined state called quark gluon plasma (QGP). The universe based on the current cosmology has evolved from an intial state of extream energy density to the present state through rapid expansion and cooling. We believe in the phase transition described by QCD at the early universe. The only one is experimentally the heavy ion collisions in the current technique for raising the phase transition in our laboratory. We should search and discovery the signatures of QGP with heavy ion collisions in order to understand the thermal history of our universe. The most promising probe in heavy ion collisions is expected to be an electromagnetic particle beacuase of its long life time, that is, a large mean free path in the reaction regime strongly interacting. The electromagnetic partielces can escape from the reaction region and carry pure information on it. We focus on the emission of electromagnetic particles in heavy ion collisions. Our purpose is to measure electromagnetic particles at the range of energy from several hundred MeV to several GeV with high accuracy. A large amount of particles is ,however, produced in ultra relativistic heavy ion collisions compared to elementary reactions such as electron-positon and proton-antiproton in a unit solid angle, further, almost all of produced electromagnetic particles are not probes which we expected but background photons originated from hadronic decay process of neutral mesons. We require the electromagnetic calorimeter with high granularity in order to measure electromagnetic particles accurately in such a high particle multiplicity environment. It is essential to develope calorimeter material as scintillators with the small Moliere radius because the position resolution strongly depends on the Moliere radius as long as we fix the total volume of the calorimter. We also request the calorimeter with high energy resolution to efficiently identify a particle which decayed into electromagnetic particles. It is important to increase the amount of scintillation light and to improve its uniformity and transparency because the energy resolution relys on these characteristics. In the next generation programme , the center-of-mass energy per neucleon,$\sqrt{s_{NN}}$, will be 5.5 [TeV]. A number of produced particles at $\sqrt{s_{NN}}$ =5.5 [TeV] is about 10 times large as in the current experiments at $\sqrt{s_{NN}}$ =150 [GeV] in a unit solid angle. As long as we place a calorimeter at the same distance from the collision point, we have to make the transversal size of calorimeter segments smaller at least one third than the current samllest size, 5.5×5.5 [cm^2].The high resolution calorimeter would drastically enhance the discovery potential for photons directly emitted from a hot and dense matter created in heavy ion collisions both of the current and future experiments. We made lead tungstate ($PbWO_4$ or PWO) crystals doped yttrium at Furukawa Co., Japan. We consider PWO crystals to be the best candidate for a high performance electromagnetic calorimeter because of its smallest Molière radius of 2.2 [cm] in the inorganic scintillators. We have Y-doped PWO crystals with the dimensions of 20×20×200 [mm^3]. The size is adequate for real applications.

In this study, we report the optical and scintillating properties for the Y-doped PWO crystal,

and the energy resolution for the single PWO crystal at the regime between several hundred MeV and several GeV.

Chapter 2

Principles

We explain about scintillation and electromagnetic shower. The physics processes are foundamental on our energy measurement for high energy electromagnetic particles. We also describe the PWO crystal.

2.1 Scintillation

Some transparent substances emit visible light when irradiated. Its phenomenon is called scintillation, its substance is a scintillator. The scintillation is simply interpreted as emission of extra eneries in the form of optical photons when exited states by irradiation become stable. When ionizing particles move though a inorganic crystal scintillator, free electrons, holes and electron-hole pairs are created. The carriers are captured at "color center", which is the local energy level resulting from lattice defects or regular lattice, and excite the center. The excited center emit the scintillation light and then settle down. While in scintillators of organic substances, inert gases and their liquids, ionizing partilces directly excite their constituents (atoms or molecules).

2.2 Electromagnetic shower

High energy electrons moving though matter lose their energy by bremsstrahlung and high energy photons do by electron-positron pair production. The bremsstrahlung is the photon emission resulting from charged particles decelerated by Coulomb electric field of nuclear. The electron-positron pair production is also caused by the nuclear Coulomb field. Repeated their two processes, the secondary photons and electrons multiply and expand like as"shower". The multiplication comes to an end when secondary energies are below the critical energy, E_c, because the main energy loss process become the ionization instead of the bremsstrahlung.

The characteristic unit related to the interactions in matter is called the radiation length, X_0 and the Moliere radius, R_M. The average energy loss of electrons by the bremsstrahlung is 64% of their energy in the matter with the thickness of X_0 (see eq.(2.2.2)). The probablity of the pair production is 54% where photons move though the matter with the thickness of X_0 (see eq.(2.2.5)). The electromagnetic shower transversally expands R_M across with the depth of X_0. The electromagnetic shower achieves 20 X_0 long and 3 R_M wide in the matter independently on its material.

For $E \gg m_e c^2/\alpha Z^{1/3}$;

The energy loss by bremsstrahlung, $-(dE/dx)_{brem}$, is described as eq.(2.2.1).

$$-\frac{dE}{dx}_{brem} = 4\alpha r_e^2 E \frac{N_A}{A} Z^2 \ln\frac{183}{Z^{1/3}} \equiv \frac{E}{X_0} \tag{2.2.1}$$

$$< E > \;=\; E_0 \exp(-x/X_0) \tag{2.2.2}$$

The cross section of the pair production, σ_{pair}, is written by eq.(2.2.3).

$$\sigma_{pair} \;=\; 4\alpha r_e^2 \frac{7}{9} Z^2 \ln \frac{183}{Z^{1/3}} \;=\; \frac{7A}{9N_A}\frac{1}{X_0} \tag{2.2.3}$$

$$\frac{\mu}{\rho} \;=\; \sigma_{pair}\frac{N_A}{A} \tag{2.2.4}$$

$$< I > \;=\; I_0 \exp(-\frac{\mu}{\rho}x) \;=\; I_0 \exp(-\frac{7}{9}\frac{x}{X_0}) \tag{2.2.5}$$

The Moliere radius, R_M, is often defined as eq.(2.2.6)

$$R_M \;=\; X_0 E_s / E_c \tag{2.2.6}$$

$$E_c \;=\; \frac{610\,[\mathrm{MeV}]}{Z + 1.24} \tag{2.2.7}$$

$$E_s \;=\; m_e c^2 \sqrt{4\pi/\alpha} \;=\; 21.2052\,[\mathrm{MeV}] \tag{2.2.8}$$

All variables have usual meanig especially without excuse.

2.3 Electromagetic calorimeter

The amount of the scintillation light initiated by an electromagnetic shower is proportional to its incident energy in the case that the material is enough large to contain the expanding shower. We read out the total scintillation light so that the incident energy can be measured. The calorimetry is how to meausre energy, and the practical instrument is called electromagnetic calorimeter. The energy resolution, σ/E, of calorimeters depends on the incident energy and can be usually parametrized as eq.(2.3.1);

$$\frac{\sigma}{E} \;=\; \sqrt{\left(\frac{a}{\sqrt{E}}\right)^2 + b^2} \tag{2.3.1}$$

$$\equiv\; \frac{a}{\sqrt{E}} \oplus b \tag{2.3.2}$$

where E is the incident energy in unit of GeV, a is the stochastic coefficient which reflects statistical fluctuations of shower development and scintillation light, b is the constant term which is influenced by calibration errors, nonuniformies and nonlinearities in instruments, and incomplete shower containment, and electronic noises. We often express eq.(2.3.1) as eq.(2.3.2) where $\oplus$ denotes the squre root of the quadratic sum.

The two dimensional hit position for the calorimetr is often estimated via center of gravity, (x_G,y_G), expressed as eq.(2.3.3).

$$x_G \;=\; \sum_i^N E_i x_i \,/\, \sum_i^N E_i \quad , \qquad y_G \;=\; \sum_i^N E_i y_i \,/\, \sum_i^N E_i \tag{2.3.3}$$

where (x_i,y_i) is the center position of the i-th cell and E_i is the deposit energy in it. The position resolution also depends on an incident energy and can be parametrized as eq.(2.3.4).

$$\sigma_{x,y} \;=\; \frac{f}{\sqrt{E}} \oplus g \tag{2.3.4}$$

2.4 PWO crystal properties

The lead tungstate ($PbWO_4$ or PWO) crystal is a scintillator. We consider the best candidate for a high performance electromagnetic calorimeter since its small Moliere radius of 2.2 [cm] compared to other inorganic crystal scintillators as shown in Table 2.1. We also tabulated general properties of the PWO crystal in Table 2.2. In the addtion to the above, it is well known that the scintillation decay spectra of PWO consist of two component, the blue component (BC) peaking around 420 [nm] ascribed to the regular lattice center $(WO_4)^{-2}$ and the green component (GC) peaking around 500 [nm] attributed to the defect WO_3 center.

Table 2.1: Comparision to other inorganic crystal scintillators

Crystal	Radiation length [cm]	Moliere radius [cm]	Decay time [ns]	Light output [% NaI]
PWO	0.89	2.2	5∼15	1
BGO	1.12	2.4	300	15
NaI	2.59	4.5	250	100
CsI	1.85	3.8	565	40

Table 2.2: General properties of the PWO crystal

Crystal	tetragonal (a =5.5 [Å], c =12 [Å])
Structure	scheelite-type
Meting point	1123 [°C]
Density	8.28 [g/cm^3]
Radiation lengh	0.89 [cm]
Moliere radius	2.2 [cm]
Energy loss per mip[1]	13.0 [MeV/cm]
Decay time	5∼15 [ns]
Peak emission	420∼440 [nm]
Refractive index	2.3
Relative light output	1 [% NaI]
Hygroscopic	no

Chapter 3

Utilities

We mention the utilites on our studies. A photomutiplier tube is used for reading out the scintillation light. GEANT4 is the programing code with which we simulated the electromagnetic shower. REFER and KEK-PS are the experiment facilities where we peformed the beam test.

3.1 Photomutiplier tube

We selected the photomultiplier R7056 made in Hamamastu in order to efficiently and accurately count the scintillation photons from the PWO crystal, whose peak emission is 420 [nm], with size of $20\times\ 20\times\ 200$ [mm^3]. Table 3.1 shows general paramters for Hammatsu R7056.

Table 3.1: Spec for the photomultiplier (Mamamastu R7056)

Spectral response	185$\sim$650 [nm]
Wavelength of maximun response	420 [nm]
Photocathode	Bialkali (25[mm] in diameter)
Window	UV glass
Dynode	10 stages (linear focused)

3.2 Single photoelectron technique

It is most conventional to measure decay time of the scintillation light with single photoelectron technique (sometimes called conventional delayed coincidence method). In this method, we can measure the arrival time after excitation of ecah scintillation photons resulting from a single excitation. In this report, for example, we placed a ^{60}Co $\gamma-$ray source between the plastic scintillator coupled with one photomultiplier tube (PMT) and the PWO crystal coupled with another PMT. One 1.2 MeV $\gamma-$ray impinges on the plastic scintillator. The emitted scintillation light is detected by the PMT and is converted into a "start" timing pulse by a discriminator. The other 1.2 MeV $\gamma-$ray independently causes the PWO crystal to emit the scintillation light. The scintillation light is detected by the other PMT and is converted into a "stop" timing pulse by the discriminator whose threshold is set to detect single photon, however, single photoelectron as long as we use PMTs. The time between "start" and "stop" pulses is digitized by a time-to-digital converter.

3.3 REFER

REFER[1] is a device for application of relativistic electron beam, especially development of X-ray source, and for education in beam physics at Hiroshima University Venture Business Loboratory (Hi-VBL[2]). REFER consists of a storage ring and a extraction line of electron beam. The energy of electron beam is 150 MeV generated by the microtron at Hiroshima Synchrotron Radiation Center (HiSOR[3]). The storage ring with circumference of 13.7 m has an injection septum magnet and two bump magnets that inject electrons into the ring, eight bending magents that bend the beam orbit with angle of 45° and curvature of 0.75 m and that circulate the electron beam in the reference orbit, a target chamber for some application, a beam scraper and a beam absorber and an extraction kicker magnet that pertubate the beam orbit, and an extraction septum magnet which slowly (10 [Hz]) extracts the circulating electrons. The extraction line with length of 6 m has a bending magnet which guides the extracted electron beam to the extraction line and two quadrupole magnets for beam focusing. The present REFER dose not have any acceleration systems. The energy loss of electron beam is around 60 eV per revolution because of synchrotron radiation.

3.4 Monte Carlo simulation with GEANT4

GEANT[4] is a detector simulation toolkit broadly used in the field of high energy plysics. GEANT4 is the latest version decribed by C++ programing language. The GEANT simulates many interactions between particles and materials in the wide energy range by the Monte Carlo method.

3.5 KEK 12 GeV Proton Synchrotron

The KEK 12 GeV Proton Synchrotron (KEK-PS) is the accelerator constructed at KEK[5] for providing physicists with excellent beams. Two experimental hall, north and east counter halls, are ready for experiments using proton beams slowly extracted from KEK-PS. 12 GeV protons extracted to the experimental hall create the secondary particles such as pions, kaons and antiprotons by metal targets. We tabulated beam lines at the east counter hall in Table 3.2 and at the north counter hall in Table 3.3. T1 and $\pi 2$ lines in the east hall are often used for the research and development of the detector.

[1] REFER is said to be an abbreviation for “Relativistic Electron Facility for Education and Research”.
[2] http://www.vbl.hiroshima-u.ac.jp
[3] http://www.hsrc.hiroshima-u.ac.jp
[4] GEometry ANd Tracking
[5] High energy accelerator research organization in Japan

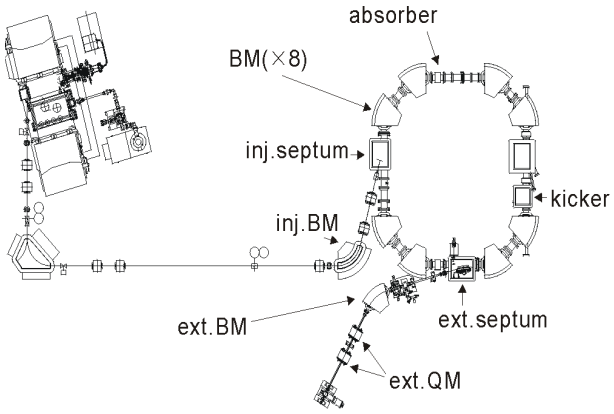

Figure 3.1: REFER

The left is the macrotron, the right is the storage ring and extraction line. 150 MeV electron generated by the macrotron is injected the storage ring in and extracted 10 [Hz].

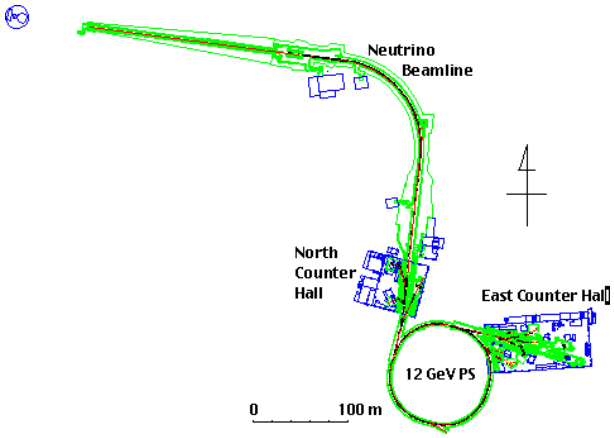

Figure 3.2: KEK 12 GeV Proton Synchrotron (KEK-PS)

12 GeV proton accelerated by PS is extracted to the north counter hall via the EP1 line, and to the east counter hall via the EP2 line. The neutrino beam line is contructed for the K2K experiment.

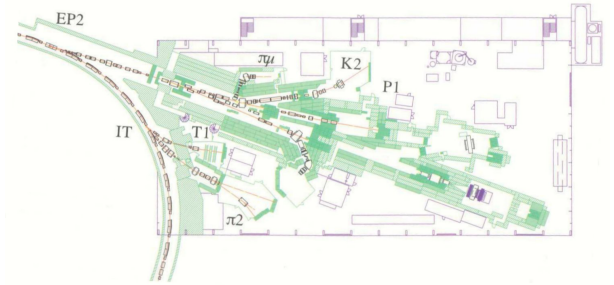

Figure 3.3: East counter hall at KEK-PS

EP2 is the extracted beam line to the east counter hall. $\pi\mu$, K2 and K3 are secondary beam lines by the external target, T1 and $\pi 2$ by the internal target (IT). P1 is the direct beam line for primary 12 GeV protons.

Table 3.2: Beam channels in the east hall

Name	Sepcification	Max momentum [GeV/c]
	Beam lines from external targets	
K2	Separated beam	2
$\pi\mu$	Unseparated beam	0.3
K3	Separated	1.1
	Beam lines from internal targets	
$\pi 2$	Unseparated	4
T1	Test beam	2
	Beam line directly from PS	
P1	Primary beam	12

Table 3.3: Beam channels in the north hall

Name	Sepcification	Max momentum [GeV/c]
K5	Separated beam	0.65
K6	Separated beam	2.0
EP1-B	Test beam	8

Chapter 4

Experiments

We address in this chapter our experiments. We measured the foundamental optical and scintillating properties (transmittance, light yield and decay time) for our PWO samples. We calibrated our photomultiplier in order to measure scintillation properties. We tested by electron and hadron beams to obtain the energy resolution.

4.1 Test samples

We have three PWO samples named PWO(A), PWO(B) the size of $20\times20\times200$[mm^3] and PWO(C) in $20\times20\times100$[mm^3]. All PWO samples were manufactured at Furukawa Co. They are made from the mixuture of lead oxide (PbO) and tangsten oxide (WO_3) uisng the Czochalski method in air atmosphere above the melting point (around 1200 °C) and the repeated (third) crystalization. They are doped yttrium ions with the concentration of 108 [at.ppm]. In addition to the PWO samples, we have one BGO crystal the size of $20\times20\times200$[mm^3] in order to compare scintillation properties.

4.2 Transmittance

Transmission spectra were measured with a spectrophotometer (Hitachi U3010). Figure 4.1 shows spectra of the longitudinal (the probing light goes through the crystal 10 cm across) and transversal (2 cm across) transmittance of PWO(C). The transmittance curve, especially longitudinal one, hollowed around the wavelength of 420 nm (blue region) by the absorption bands of residual lead oxide, so that our PWO samples looked slightly yellowish. The longitudinal and transversal cutoff wavelengths were 332 nm and 328 nm, respectively. The wavelength indicates an original absorption by the PWO crystal. Comparing the two spectra, we estimated the internal attenuation coefficient, α, described in eq.(4.2.1) by employing eq.(4.2.2).

$$T = T_0 \exp\left(-\alpha z\right) \tag{4.2.1}$$

$$\alpha = -\frac{\ln\left(T'/T\right)}{z'-z} \tag{4.2.2}$$

where T is the transmittance, z is the longidutinal thickness of the crystal. We found the magnitude of α is approximately 0.018 cm^{-1} at the wavelength of 420 nm.

4.3 Calibration for photomultipliers

We prepared a photomultiplier sensitive to one photon for reading out the scintillation light from a PWO crystal. The photomultiplier is R7056 made in Hamamtsu Co., Japan. We calibrated its

photomultiplier with a green light-emitting diode (LED) in order to estimate its multiplication for applied voltage. We placed a green LED and a photomultiplier 9 [cm] apart in a black box for room light shielding as shown in Figure 4.2. A pulse generator initiated the green LED and opened a ADC (LeCroy 2249A) gate via a translator and a discriminator. The translator converts TTL signal into NIM signal. The discriminator outputs the logic pulse when the the pulse hieght of the input signal is above its threshold. We monitored at a digital oscilloscope the pluse signal injected to the LED by the pulse generator so that we arranged the light intensity to detect the single photoelectron arriving at the photomultiplier. The signal from the photomultiplier was also digitized by the above ADC. We tested two same photomultipliers conveniently called their serial number VA0009 and VA0010.

We observed the single photoelectron as shown in Figure 4.3 with one photomuliplier (VA0009) applied to a high voltage of -1.5 [kV]. We considered it as a single photoelecton because of the fact that the peak position did not shift at all when we sapareted the LED and the photomultiplier 14 [cm] apart and then 18 [cm] apart. We searched the sigle photoelectron as varing a high voltage applied to the photomultiplier the range from -1.2 to -2.0 [kV]. We fitted with Gaussian the spectrums in which we observed the single photoelectron , and then calculated the multiplication factor called gain, G, by employing eq.(4.3.1). We repeated the same calibration with another photomultiplier (VA0010). Figure 4.4 shows gain curves of our photomultipliers against applied voltage. The open and closed circles represented the measured data for VA0010 and VA0009 photomultiplier, respectively.

$$G = \frac{(X_{spp} - X_{ped}) \times 0.25}{1.6 \times 10^{-7}} \tag{4.3.1}$$

where X_{spp} and X_{ped} are the peak channel in ADC for single photoelectron and pedestal, respectively. We call the ADC offset "pedestal". Here we apply the value of 1.6×10^{-7} as elementary charge in unit of pC. The input sensitivity of the ADC (LeCroy 2249A) is 0.25 [pC/channel].

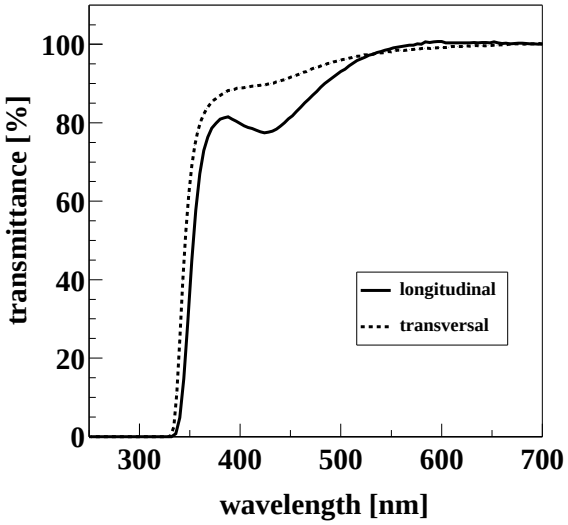

Figure 4.1: Transmission spectrums

The solid and dashed lines are the longitudinal and lateral transmission spectrums on the PWO(C) sample with the dimensions of 20× 20× 100 [mm^3]. The hallow at the blue region seems to be the absorption of the residual lead oxide.

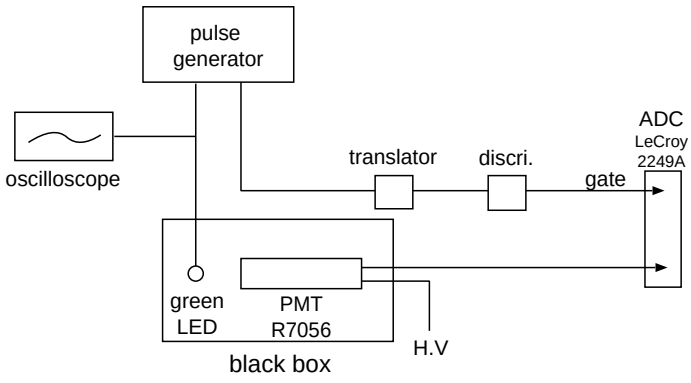

Figure 4.2: Setup for photomultiplier calibration

The green LED is initiated by the pulse generator. The distance between the LED and PMT is 9 [cm].

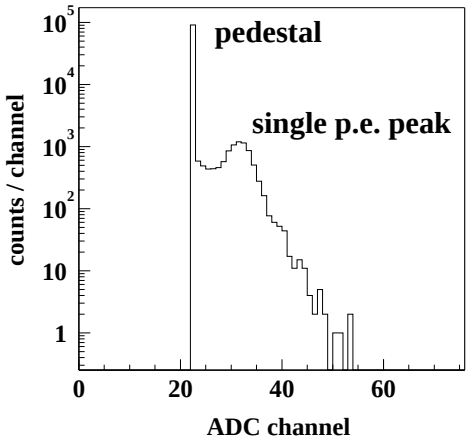

Figure 4.3: Typical ADC spectrum for single photoelectron
The high voltage of -1.5 [kV] is applied to the photomultiplier (Hamamatsu R7056:VA0009). The peak position is 22 [ch] for the pedestal, 31 [ch] for the single photoelectrons.

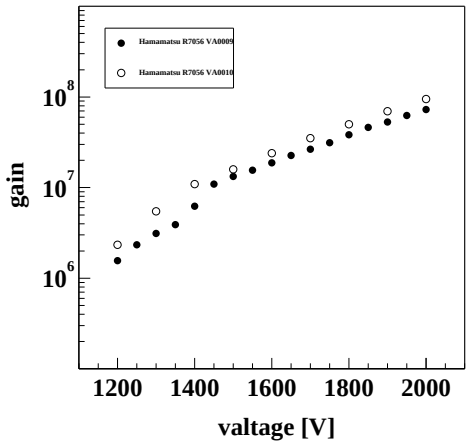

Figure 4.4: Gain curves
For the photomultiplier (Hamamatsu R7056). The closed and open circles are VA0009 and VA0010, respectively. $G \sim 10^7$ for -1.5 [kV].

4.4 Measurements of scintillation properties

We tested two PWO samples, PWO(A) and PWO(B), with the size of $20\times20\times200$[mm^3] irradiated by γ-rays from a ^{60}Co source for measurements of scintillation properties. We simultaneously investgated light yield and decay time in the setup shown in Figure 4.5. We placed the ^{60}Co source between the PWO sample coverd with an aluminum foil and a plastic scintillator in a black box. The aluminum foil prevents the scintillation light from escaping. The PWO crystal optically coupled with a photomultiplier (Hamamastu R7056). The plactic scintillator as a trigger coupled with a photomultiplier (Hamamastu H2431). We splited the output signal from the photomultiplier. One signal was digitized by ADC (LeCroy 2249A) for measuring light yield. Another was converted into timing pulses by a discriminator then digitized by TDC (REPIC RPC060) for obtaining a decay time spectrum. The signal from the plastic scintillator played a role of a ADC gate and a TDC start timing pulse. We used one of the slited signals from the PWO crystal as a TDC stop timing pulse. We also tested one BGO samples, same size as our PWO samples, for comparision. In this test, we read out the scintillation light from the crystal with the VA0009 photomultiplier. The high voltage of -1.9 [kV] was applied to the VA0009 in the PWO sample, -1.2 [kV] in the BGO sample. The period of the ADC gate was tuned with 200 [ns].

4.4.1 Light yield

Figures 4.6 of (a) and (b) show obtained spectrums for γ-ray from a ^{60}Co with the PWO samples after the calibration was made by employing eq.(4.4.1). The typical raw ADC spectrum for the PWO sample is shown in the top of Figure 4.7. We converted the ADC channel into the number of photoelectrons beacuase the ADC channel for observed single photoelectron peak was consisted with our calibration for photomultipliers. We observed a photopeak for ^{60}Co, which correponds to 1.2 [MeV] deposited at the PWO crystal. The ^{60}Co spectrums were fitted on Gaussian with exponential background. The obtained mean is the number of photoelectrons for ^{60}Co photopeak, N_0. By calculating accroding to eq.(4.4.2), the light yields were found to be 4.5 and 8.2 photoelectrons per deposit energy in unit of MeV ([p.e./MeV]) for PWO(A) and PWO(B), respectively.

$$N_{pe} = \frac{X[\mathrm{ch}] - X_{ped}[\mathrm{ch}]}{X_{spp}[\mathrm{ch}] - X_{ped}[\mathrm{ch}]} \tag{4.4.1}$$

where N_{pe} is the number of photoelectrons intiated by γ-rays from a ^{60}Co radioisotope, X is the ADC channel, especially, X_{spp} and X_{ped} correspond to the single photoelectron peak and pedestal, respectively.

$$LY = \frac{N_0}{1.2[\mathrm{MeV}]} \tag{4.4.2}$$

where LY is the light yield, N_0 is the number of photoelectrons for the ^{60}Co photopeak, 1.2 MeV is the energy deposited by ^{60}Co γ-rays.

Figure 4.6 of (c) shows the ^{60}Co spectrum for the BGO crystal after the calibration. The ADC channel was calibrated by eq.(4.4.3). Unlike the PWO crystal, we did not observe the single photoelectron peak and the photopeak together because the BGO sample was a large light output for γ-rays from a ^{60}Co source. We fitted the spectrum around the ^{60}Co photopeak with Gaussian, and obtained the N_0 for the BGO crystal. The light yield for the BGO sample was found to be 404 [p.e./MeV] by eq.(4.4.2).

$$N_{pe} = \frac{2\times(X[\mathrm{ch}] - X_{ped}[\mathrm{ch}])\times 0.25[\mathrm{pC/ch}]}{1.6\times10^{-7}[\mathrm{pC}]\times G} \tag{4.4.3}$$

Here the variables are the same meaning as above equations. The factor of 2 is required because we split the signal outputed from the crystal (see Figure 4.5).

4.4.2 Decay time

We measured decay time with the single photoelectron technique. To guarantee its method against our measurement of decay time, we analytically extracted events for single photoelectrons from all events by using the single photoelectron peak in the ADC spectrum as shown in Figure 4.7. In addition to the analysis, for the BGO sample, we had to physically mask the crystal by the sheet with a pinhole because the light output of the BGO crystal was large as much as that of the PWO crystal. We limited to one the average scintillation photons from the crystal which was counted during the period of the ADC gate. Without the limitation, we will consider the fastest photon in the photons arriving at the photomultiplier among the ADC gate as the TDC "stop" timing pulse so that we can not obtain a correct decay spectrum.

The typical raw TDC spectrum for the PWO sample is shown in the bottom of Figure 4.7. We converted the TDC channel, Y, into time, t, in [ns] by eq.(4.4.4). After selecting single photoelectron events, we omitted both under and over flows. We defined the point for maximum count as t_0. We set t_0 to 0 [ns].

$$t = Y[\text{ch}] \times 0.025[\text{ch/ns}] - t_0 \tag{4.4.4}$$

Figure 4.8 of (a), (b) and (c) shows the scintillation decay time spectrums for PWO(A), PWO(B) and BGO, respectively after the calibration. The region at $t < 0$ in the spectrum indicates the rise up time ascribed to the plastic scintillator, the tail at $t > 0$ shows the decay time for the crystal. The obtained decay time spectrums were well fitted at $t \geq 0$ with eq.(4.4.5) as a function of time in PWO crystals,

$$f(t) = (N_f/\tau_f)\exp(-t/\tau_f) + (N_s/\tau_s)\exp(-t/\tau_s) \tag{4.4.5}$$

with eq.(4.4.6) in a BGO crystal,

$$g(t) = (N/\tau)\exp(-t/\tau) \tag{4.4.6}$$

where N is the number of scintillation photons reaching a PMT, τ is the decay time, subscripted s and f indicate the slow and fast componets, respectively. The total intensity corresponds to $N_f + N_s$ in the case of two components. The decay time of scintillation light can be parametrized; τ_f = 1.7 ns (for 30% of the total intensity), τ_s = 5.6 ns (70%) in PWO(A), τ_f = 1.2 ns (17%), τ_s = 6.0 ns (83%) in PWO(B), τ = 185 ns in BGO.

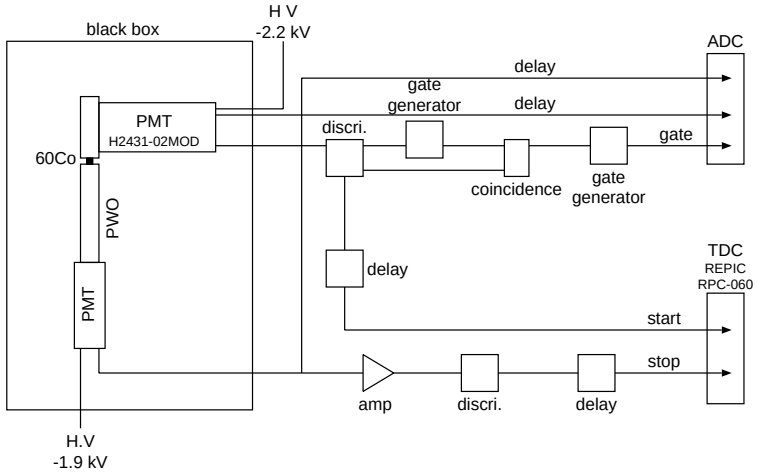

Figure 4.5: Setup for measuremts of light yield and decay time

4.5 Response to comsic-rays

To ensure the difference of light yield between PWO(A) and PWO(B), we tested by cosmic particles penetrating though the crystal. Sketched in Figure 4.9, we piled up two PWO crystals coupled with a photomultiplier (Hamamatsu R7056) and placed two same triggers symmetrically above and below the crystals. The PWO(A) sample was optically contacted with the VA0010 photomultiplier, the PWO(B) with the VA0009. The two samples were coverd with an aluminum foil, except for the face of contact with the photomultiplier. The triggers have a plastic scintillator of 1×1 [cm^2] optically coupled though a light guide of 10 [cm] long with a photomultiplier (Hamamatsu R3478). The cosmic particles deposit their energies equally in both of the PWO(A) and PWO(B) samples in such a geometry. The apparatus was set in a black box for shading the room light.

The blank and shadow in Figures 4.10 correspond to the response of cosmic-rays for PWO(A) and PWO(B), respectively. We calibrated the ADC channel by employing eq.(4.5.1). The spectrums were fitted with Gaussin, and the light output was 160 ± 46 photoelectrons for PWO(A) and 305 ± 68 ones for PWO(B). The number of photoelectrons from PWO(B) was two times as large as that of PWO(A). We assumed both samples were given the same energy by cosmic particles. The light yield of PWO(B) was also two times as large as that of PWO(A) like as the measurement with γ-ray from a ^{60}Co source. We found that cosmic particles deposited 36 ± 10 [MeV] in PWO(A) and 37 ± 8 [MeV] in PWO(B), applying 4.5 [p.e./MeV] for PWO(A) and 8.2 [p.e./MeV] for PWO(B). Our assumption was satisfied. The cosmic particle traverse the crystal 2.8 [cm] across in this setup by calculating with the value of its energy loss for the PWO crystal, 13 [MeV/cm].

$$N_{pe} = \frac{(X[\mathrm{ch}] - X_{ped}[\mathrm{ch}]) \times 0.25[\mathrm{pC/ch}]}{1.6 \times 10^{-7}[\mathrm{pC}] \times G} \tag{4.5.1}$$

Here the variables are the same meaning as above equations.

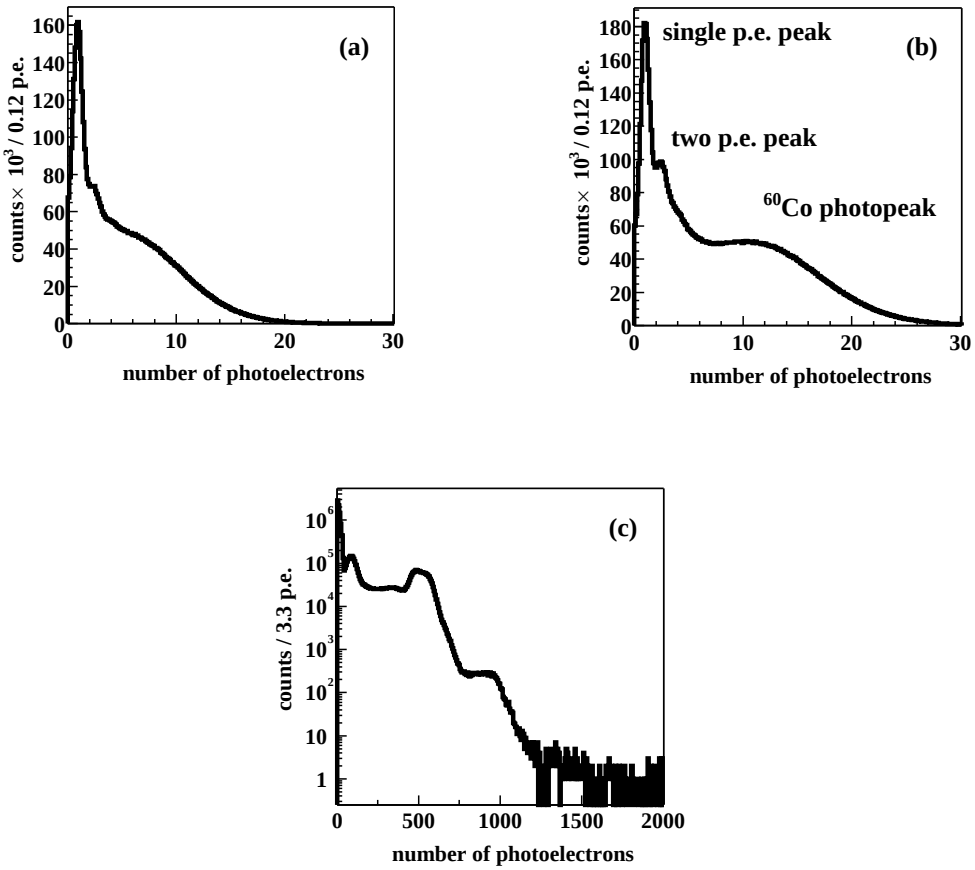

Figure 4.6: ^{60}Co spectrums
The figures of (a), (b) and (c) show PWO(A), PWO(B) and BGO, respectively. The number of photoelectrons for ^{60}Co photopeak, whose deposit energy is 1.2 [MeV], is 5.4, 9.8 and 485.

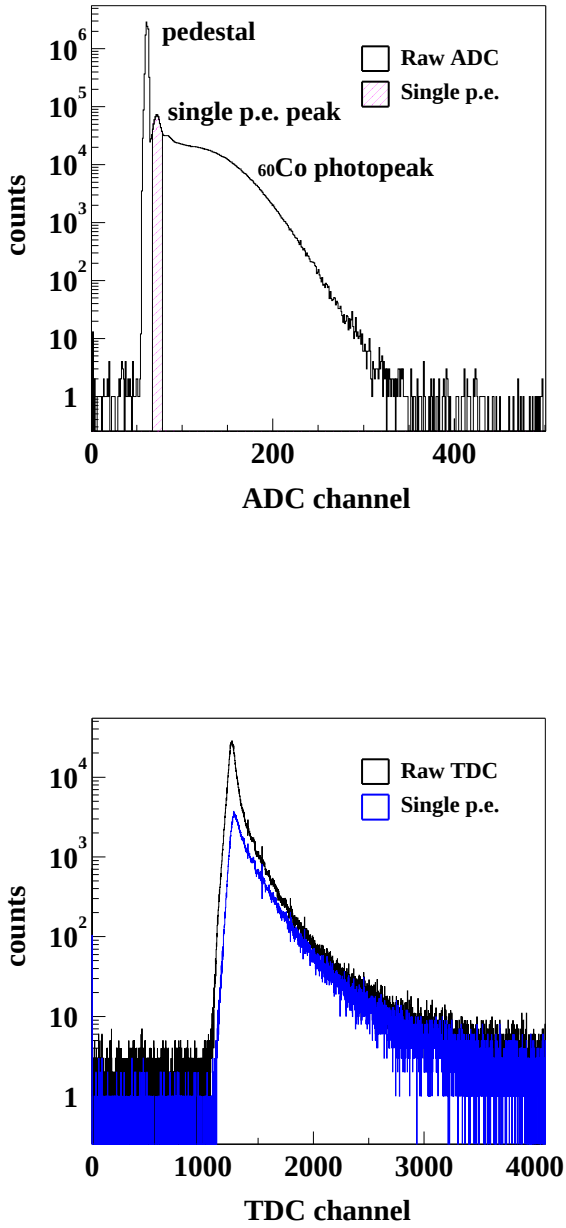

Figure 4.7: Analytical single photoelectron technique
The top is a typical ADC spectrum for PWO(A) with VA0009 (-1.5 [kV]) in which the shadow region is considered as single photoelectrons. The bottom is a typical TDC spectrum. With the ADC cut, single photoelectron events are selected such as the blue spectrum.

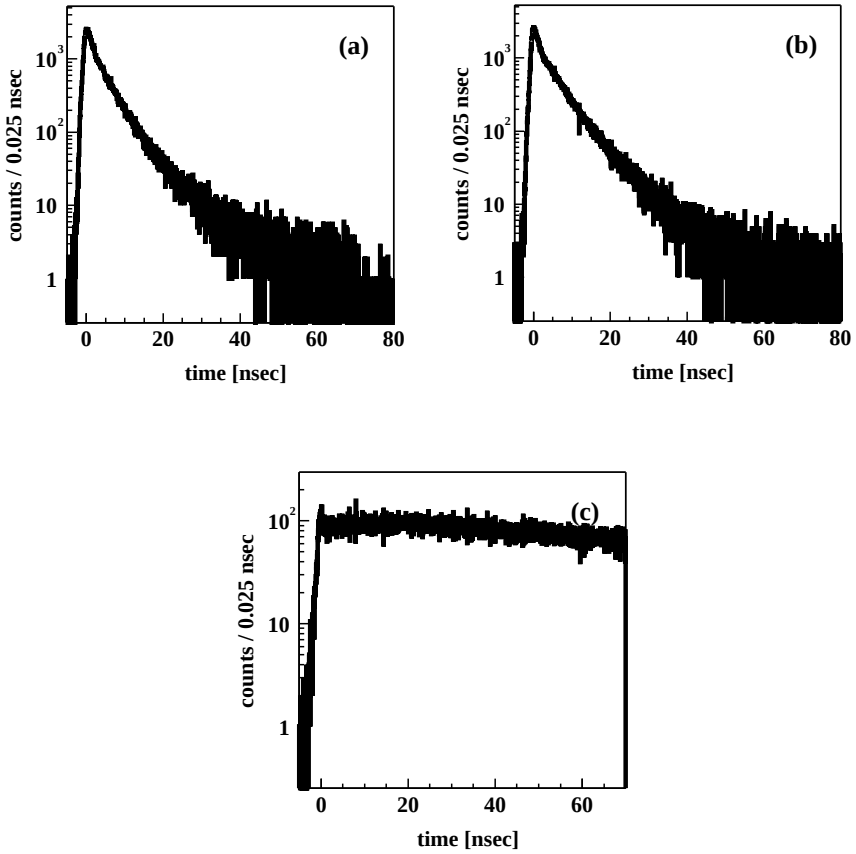

Figure 4.8: Scintillation decay curves
The figures of (a), (b) and (c) correspond to PWO(A), PWO(B) and BGO, respectively. The tail at $t \geq 0$ indicates the decay of scintillation light.

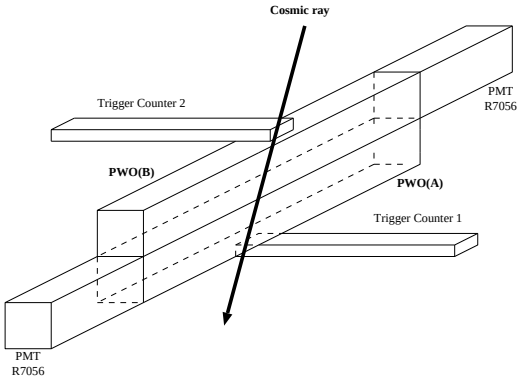

Figure 4.9: Setup for cosmic ray test
Two PWO crystals are piled up with two triggers above and below them. The ADC gate is open when a cosmic particle traverses two triggers across. The scintillating area of the trigger is 1×1 [cm^2].

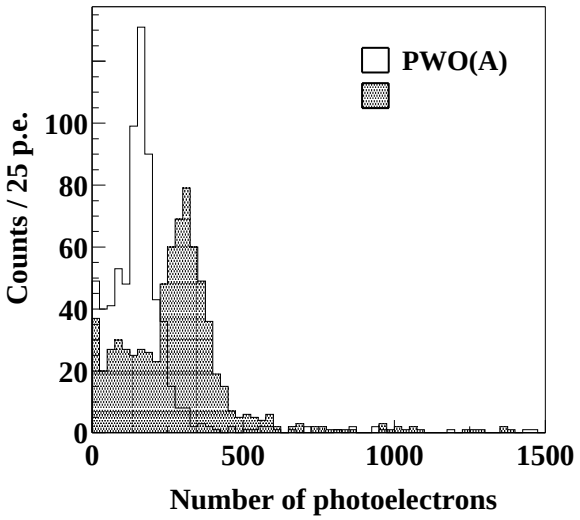

Figure 4.10: Response to cosmic particles
The blunk and shadow show the spectrum for PWO(A) and PWO(B), respectively. The light output of PWO(B) is two times large as that of PWO(A). By employing the measured light yield with a ^{60}Co source, the deposit energy is about 37 [MeV] for both crystals.

4.6 Beam tests

We performed two beam tests at REFER (Hi-VBL) and KEK-PS (KEK). The energy resolution was obtained in incident energy of 150 MeV, 1 GeV, 2 GeV and 3 GeV.

4.6.1 150 MeV electron beam at REFER

We arranged the setup shown in Figure4.11 in front of the extraction duct. The electron beam longitudinally impinged on the 20×20 [mm^2] face of the PWO crystal. We placed a collimater and two triggers between the duct and the crystal. The triggers have a plastic scintillator of 1×1 [cm^2] optically coupled though a light guide of 10 [cm] long with a photomultiplier. The collimater is a lead block with a hole of 5 [mm] in diameter and 5 [cm] long. The signal from photomulipliers was digitized like the measurents of scinitllaion properties. We applied the photomultiplier coupled with the PWO sample to the high voltage of -1.2 [kV].

Figure4.12 shows the deposit energy distribution for 150 MeV electron incident on PWO(B) sample after energy calibration was made. In the energy calibration as eq.(4.6.3), we converted the values of ADC channel, X, into the ones of energy, E_{dep}, emplying the light yield which was measured for our samples, LY.

$$E_{dep}[\mathrm{MeV}] \;=\; \frac{(X[\mathrm{ch}]-X_{ped}[\mathrm{ch}])\times 0.25[\mathrm{pC/ch}]}{1.6\times10^{-7}[\mathrm{pC}]\times G\times LY[\mathrm{p.e./MeV}]} \tag{4.6.1}$$

The first peak shown in Figure4.12 is considerd one incident electron. The second peak corresponds to two incident electrons during the ADC gate with the period of around 200 [ns]. We fitted the fisrt peak with Gaussian, then calculated using its mean and sigma. The deposit energy was found to be 116 [MeV] for one electron, 231 [MeV] for two electrons. The energy containment was 77 % of total incident energy, the energy resolution was 14 % in the single crystal. It is natural that the single PWO crystal with the lateral dimensions of 2×2 [cm^2] ($\sim1R_M$) can not contain the total incident electron energy beacause an electromagnetic shower tranversaly expands across three times as its Molière radius of 2.2 [cm]. However, the PWO crystal 20 [cm] long ($\sim20X_0$) can prevent the electromagnetic shower from escaping longitudinally. The energy resolution is much influenced by the flactuation of the energy leakage.

4.6.2 Unseperated beam at KEK$-$PS

We participated in the T496 experiment, which is one of the programme for detector test at the KEK, in order to measure electrons of several GeV and to observe response to hadrons with our PWO samples. The T496 experiment performed at $\pi2$ beam line of the east counter hall in KEK-PS. The $\pi2$ beam is an unseparated beam ,that is, includes electrons, pions, protons, kaons and deuterons. We show in Figure4.13 the special setup for the test of our PWO calorimeter in T496. We identified electrons with two gas Čerenkov counters and distinguished pions, protons and other hadrons with start and stop counters by time of flight. We guaranteed the beam direction against the calorimeter with a veto counter and defining ones. We determined under the beam momentum of ±3, ±2 and ±1 [GeV/c] where the sign indicates an electromagnetic charge of the particle.

We observed that the single PWO crystal stopped protons with the momentum of 1 [GeV/c] shown in Figure 4.14, in other words, protons of 1 [GeV/c] deposited their total kinetic energies 432 [MeV] calculated as eq.(4.6.4) at the crystal. The peak position of the energy deposit for stopped protons with the momentum of 1 [GeV/c] was calibrated to be 432 [MeV] according to the kinematics. We found the conversion factor by eq.(4.6.2), and converted the ADC channel

into the energy by eq.(4.6.3).

$$C_A[\text{MeV/ch}] = \frac{432[\text{MeV}]}{X_{stp}[\text{ch}] - X_{ped}[\text{ch}]} \quad (4.6.2)$$

$$E_{dep}[\text{MeV}] = (X[\text{ch}] - X_{ped}[\text{ch}]) \times C_A[\text{MeV/ch}] \quad (4.6.3)$$

where C_A is the conversion factor from the ADC channel into deposit energy, X_{stp} is the the ADC channel for the stopped proton peak, and the others are the same meaning above equations. C_A =3.26 [MeV/ch] for -0.8 [kV] applied to the photomultiplier (Hamamatsu R7056:VA0009), C_A =28.9 [MeV/ch] for -0.6 [kV], respectively.

Figure 4.15 is spectrum for pion and proton of 3 [GeV/c] penetrating the calorimeter longitudinally after the energy calibration. The deposit energies were 210 [MeV] for pion and 230 [MeV] for proton. We took seven data sets for electron and positron in total with the PWO(B) sample as shown in Table 4.1. Figure 4.16 shows spectrums for positorons/electrons of 1, 2 and 3 [GeV]. The obtained spectrums for positrons/electrons were fitted with Gaussian at the range between $0.7E_{inc}$ and E_{inc} (E_{inc} is the incident energy) so that the lower tail was truncated. The average of the energy containment was found to be 77 % of total incident energy for positron, 81 % for electron. The energy resolution in the single PWO crystal was found to be 6.5% and 8.8% for 1 GeV positron incident, 8.9% for 1 GeV electron incident, 8.3% for 2 GeV positron, 5.0% and 6.5% for 2 GeV electron, 5.0% for 3 GeV electron,respectively (see Table 4.1). We ploted their experimental values in Figure 5.3. The resolution is deteriorated in case that an incident particle dose not hit longitudinally the center of the crystal face because the fluctuation of energy leakage increases.

$$E_k = \sqrt{p^2 + m^2} - m \quad (4.6.4)$$

where E_k is the kinetic energy, m is the mass and p is the momentum of a particle.

Table 4.1: Data sets

run number	PMT voltage [$-$kV]	incident e^+/e^-	resolution [%]	containment [%]
1161	0.8	1GeV e^+	6.5	78
1241	0.6	2GeV e^+	8.3	76
1242	0.6	1GeV e^+	8.8	76
1243	0.6	3GeV e^-	5.2	81
1244	0.6	2GeV e^-	5.0	82
1245	0.6	2GeV e^-	6.5	82
1252	0.6	1GeV e^-	8.9	80

The run number is assigned by T496 collaboration.

Particle identification

We identified pions, kions, protons and deuterons by comparing two values. One is the difference of measured time of flight, Δt_{tof}, described by eq.(4.6.5) and another is the difference of calculated time of flight, $\Delta t'_{tof}$ by eq.(4.6.6).

$$\Delta t_{tof} = C_T(Y_1 - Y_2) \quad (4.6.5)$$

where C_T is the conversion facotr from TDC channel to time in ns. Y_1 and Y_2 are distinguishable peak channels in the TDC spectrum.

$$\Delta t'_{tof} = \left(\frac{1}{\beta_1} - \frac{1}{\beta_2}\right)\frac{L}{c} \quad (4.6.6)$$

where β is the relativistic varialbe described by eq.(4.6.7), c is the light velocity in vacuum and L is the distance between the start and stop counters.

$$\beta = \left(1 + \left(\frac{m}{p}\right)^2\right)^{-1/2} \tag{4.6.7}$$

Table 4.2 shows the clculated values for the T496 experiment.

Table 4.2: Calculated the difference of the time of flight in TDC ch

	1 [GeV/c]	2 [GeV/c]	3 [GeV/c]
πK	61	16	7
πp	211	60	27
πd	613	200	96
Kp	150	44	20
Kd	551	184	89
pd	402	141	69

The values are calculated using C_T =0.025 [ns/ch], L =4.538 [m], for the combination of pion (π), kaon (K), proton (p) and deuteron (d) with the momentum of 1, 2 and 3 [GeV/c].

Figure 4.17 shows the typical raw TDC spectrum of the start counter 1. We separated pions, kaons, protons and deuterons by Table 4.2, taking into account the time resolution of the start and stop counters. However, in case that the beam momentum set a negative value, we observed only negative pions in the TDC spectrum of the start counter. In such a case, we compared the TDC peak position for the positive momemtum to that for the negative one because the time of flight is same at the same mass and momentum.

We identified electrons with the gas (CO_2) Čerenkov counter. The gas Čerenkov counter emits the Čerenkov light when a particle is above the Čerenkov threshold velocity (eq.(4.6.8)), and dose not when the particle below the velocity. In the T496 experiment, we arranged the CO_2 gas pressure in order to distinguish between positrons/electrons and hadrons.

$$\beta_{th} = 1/n \tag{4.6.8}$$

where β_{th} is the Čerenkov threshold velocity, n is the reflective index.

Figure 4.18 shows the typical ADC spectrum of the gas Čerenkov counter. The pedestal corresponded to hadrons. The yellow region (upper region) was considered the signal attributed to positrons/electrons because few Čerenkov light was emitted for the hadrons with high momentum, although the arrangement of the gas pressure.

Figure 4.19 shows the typical ADC spectrums of the PWO calorimeter. We extracted positron/electron events from all events by the above identification with the gas Čerenkov. The pion and proton events were obtained using both the TDC peak position of the start counter and the ADC pedestal of the gas Čerenkov counter.

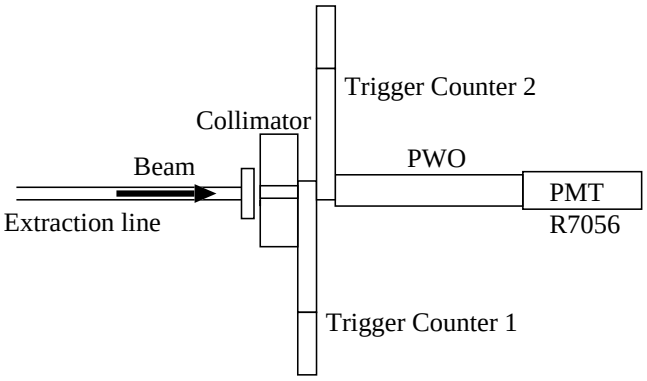

Figure 4.11: Setup for the beam test at REFER
The extraction duct is 4 [cm] in diamter, the collimater is the size of 5 [cm] $\times$ ϕ0.5 [cm]. The crystal is placed along the extraction line. The triggers are perpendicular to the extraction line.

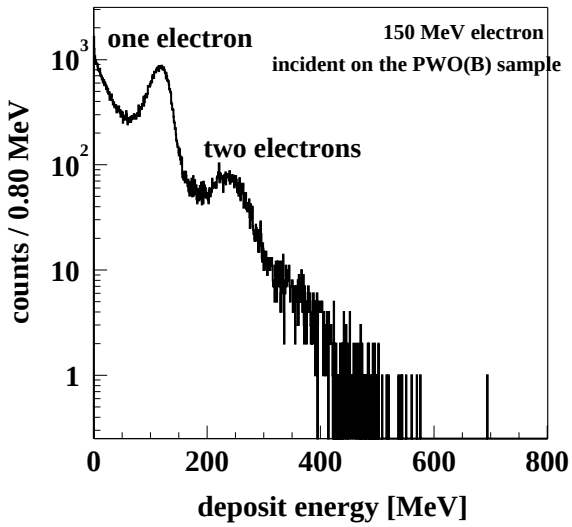

Figure 4.12: Deposit energy distribution for 150 MeV electron
150 MeV electron incident on the PWO(B) sample. The first peak is 116 [MeV] for one electron and the second peak is 231 [MeV] for two electorns incident simultaneously. The energy containment is 76 %, the energy resolution is 14 %.

Figure 4.13: Setup for PWO calorimeter test in T496 experiment
The unseparate beam (pion, kaon, proton and electron) with the momemtum of ± 1, ± 2 and ± 3 [GeV/c]. The start counters separate hadrons by time of flight, and the gas Cerenkov counters identify electrons. The veto and two defining counters guarantee the beam direction against the PWO calorimeter. The distance between start counters is 4.538 [m].

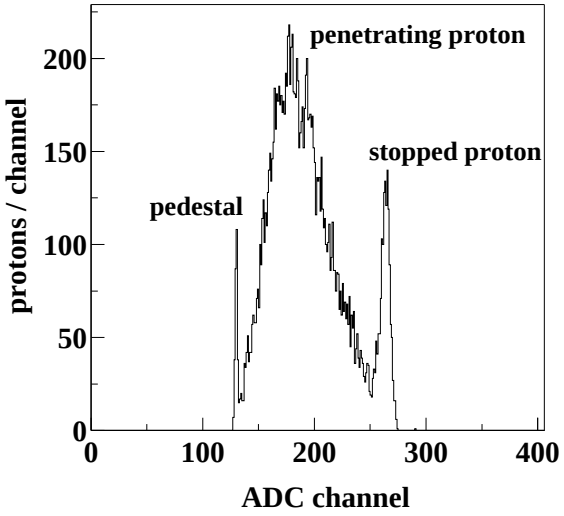

Figure 4.14: Special ADC spectrum of the PWO calorimeter for 1 GeV/c incident protons
The proton spectrum is extracted from the raw ADC spectrum with the identification by time of flight in the run 1161. Some protons penetrate the crystal , others stop in the crystal. The peak position is 130 [ch] for pedestal, 263 [ch] for stopped protons.

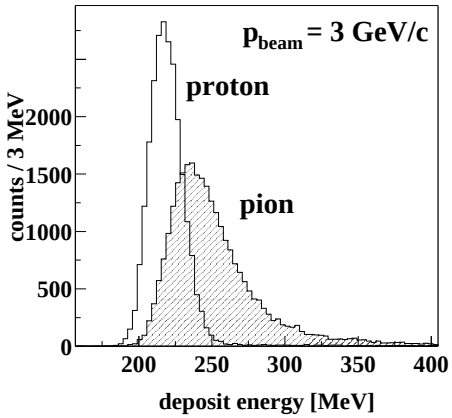

Figure 4.15: Deposit energy distribution for proton and pion
The spectrums are obtained from the ADC measured the PWO calorimeter after the energy calibration. The pion and proton are separated by time of flight. The beam momentum is 3 [GeV/c] in the run 1159. The peak position is 210 [MeV] for protons, 230 [MeV] for pions.

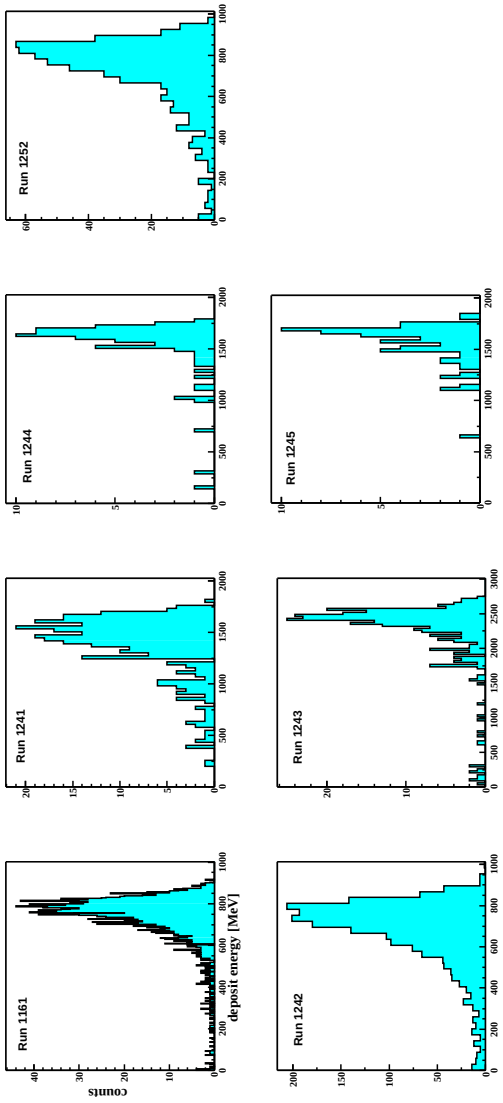

Figure 4.16: Deposit energy distribution for electrons
For 1, 2 and 3 GeV electron or positron incident on the PWO(B) sample. The spectrum were fitted with Gaussina at the range between 0.7 and 1.0 [GeV] for 1 GeV incident, 1.4 and 2.0 [GeV] for 2 GeV incident, 2.1 and 3.0 [GeV] for 3 GeV. The obtained values are shown in Table 4.1.

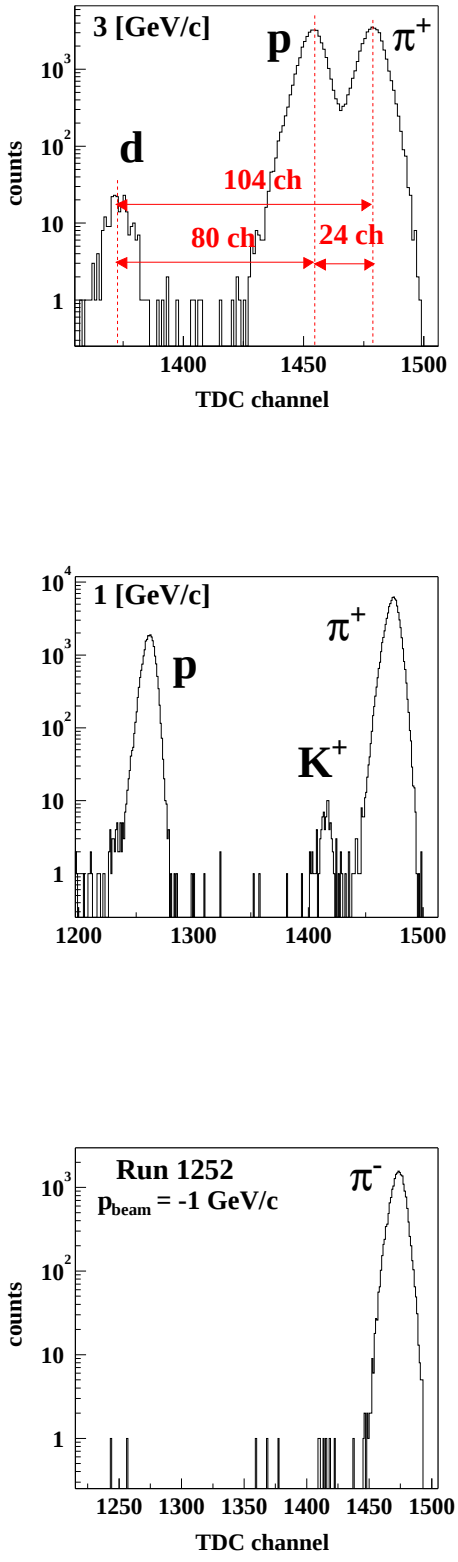

Figure 4.17: Typical TDC spectrums of start counter 1
The top is in 3 GeV/c momentum, the middle is in 1 GeV/c momentum and the bottom is in −1 GeV/c momentum. The hadrons are separated with the difference of time of flight.

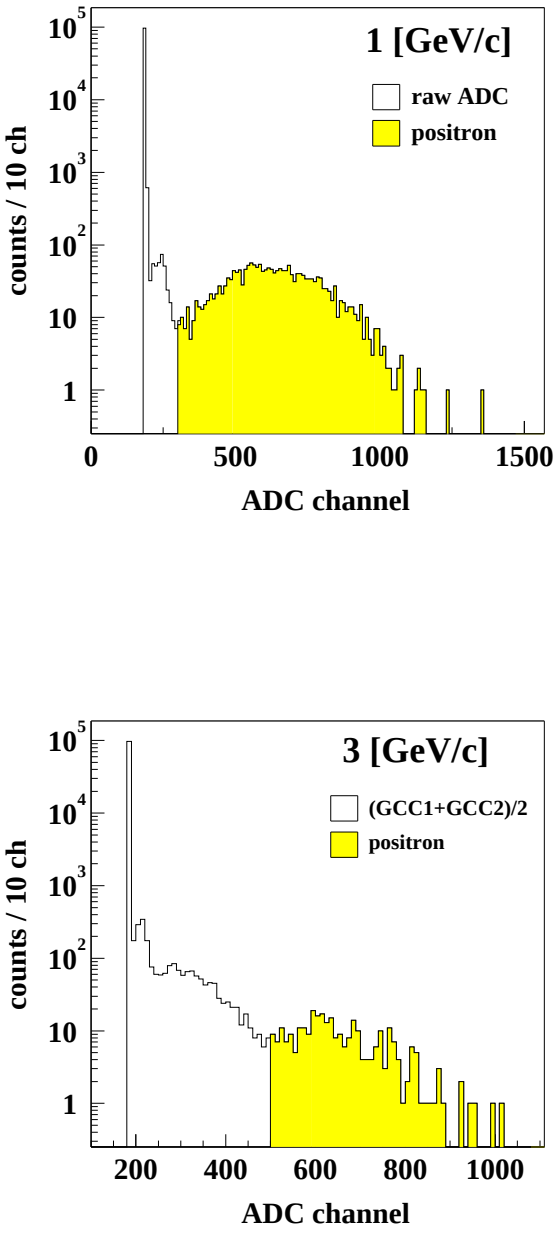

Figure 4.18: Typical ADC spectrums of gas Cerenkov counter
The top is in 1 GeV/c momentum, the bottom is in 3 GeV/c momentum. The yellow region indicates the positron events. In the negative momentum, the same region shows the electron events. The pedestal correspond to hadrons. The pedestal is 200 [ch], the cutoff point is 300 [ch] for 1 GeV/c momentum, 500 [ch] for 3 GeV/c momentum.

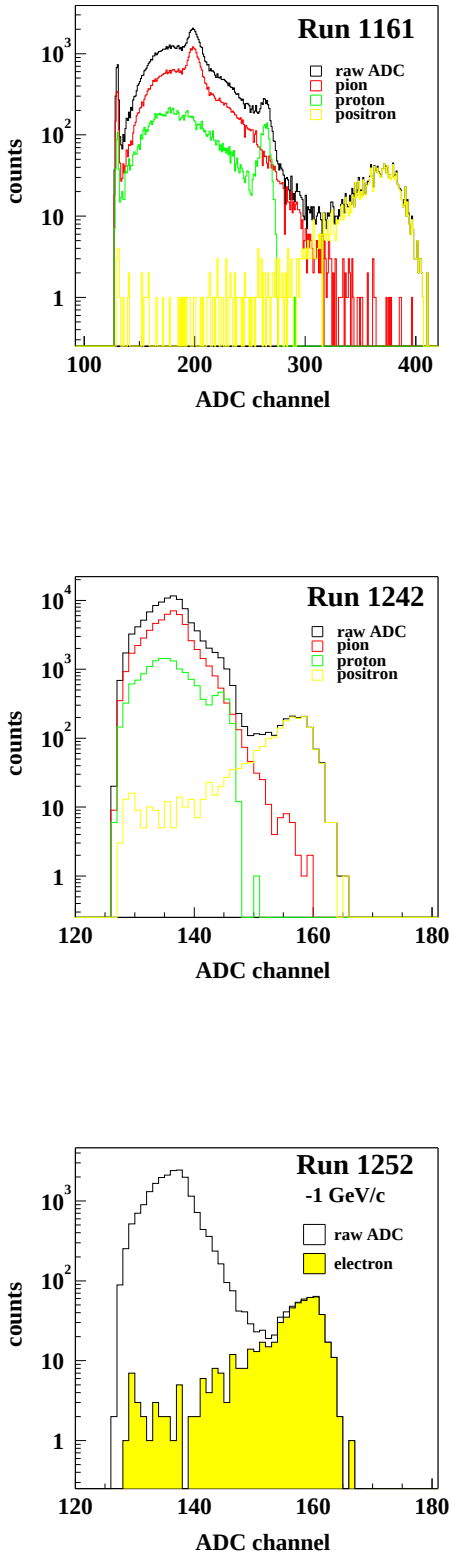

Figure 4.19: Typical ADC spectrums of PWO calorimeter
The top and middle are in 1 GeV/c momentum incident, the bottom in −1 GeV/c momentum. The particle identification is performed as above description.

Chapter 5

Discussion

We discuss the energy resolution for the PWO crystal. We parametrize the energy resolution by eq.(2.3.1) on both the experiment and simulation. We tried to compare the stochastic term between the experiment and simulation.

5.1 Energy resolution

We parametrized the measured energy resolutions at two beam tests by eq.(2.3.1). By fitting the data as shown in Figure 5.3, the coefficients were found to be a =5.4%, b =4.6%.

5.2 Simulation

We simulated with the GEANT4 code the electromagnetic shower initiated by electron incident on the PWO crystal with the incident energy of 0.15, 0.50, 1.0, 1.5, 2.0, 2.5 and 3.0 [GeV], respectively as shown in Figure 5.2. The obtained spectrums were well fitted with Gaussian at the full range. The average energy containment was 75 %. The simulated result of energy resolution can be expressed by eq.(5.2.1) for the single PWO crystal as shown in Figure 5.3.

$$\frac{\sigma_{1\times1}}{E} = \frac{4.6\%}{\sqrt{E}} \oplus 1.7\% \tag{5.2.1}$$

In addition to the above, the simulation results of energy resolution show that the energy resolution will be up to $1.8\%/\sqrt{E}$ with nine PWO crystals arranged in a 3×3 matrix as shown again in Figure 5.3. The containment will be 92 %.

5.3 Comparision of experiment to simulation

The relationship of the stochastic term between the experiment and the simulation is described as eq.(5.3.1) because we do not implement in the simulation code the fluctuation of scintillation light.

$$a_{exp} = a_{sim} \oplus a_{pe} \tag{5.3.1}$$

$$a_{ap} = \sqrt{\frac{F}{LY}} \tag{5.3.2}$$

$$F = 1 + \frac{1}{\delta_1} + \frac{1}{\delta_1\delta_2} + \cdots + \frac{1}{\delta_1\delta_2\cdots\delta_n} \tag{5.3.3}$$

where a_{exp}, a_{sim} and a_{pe} express the stochastic terms described by eq.(2.3.1) for the experiment, the simulation and the photostatistics. The stochastic term for the photostatistics is

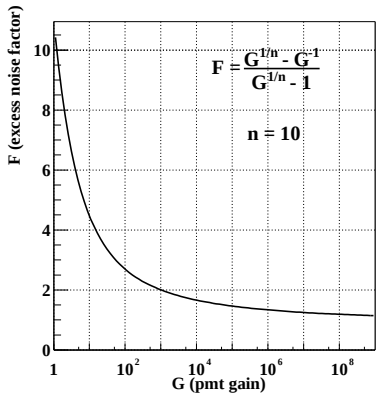

Figure 5.1: Excess noise factor for photomulitiplier gain

often expressed by eq.(5.3.2). LY is the light yield, F is the excess noise factor written by eq.(5.3.3). δ_i is the secondary emission yield of i-th dynode for a photomultiplier. Assuming $\delta_1 = \delta_2 = \cdots = \delta_n \equiv \delta$, $G = \delta^n$ where G is the photomultiplier gain and n is the number of dynode stage, therefore,

$$F = \frac{G^{1/n} - G^{-1}}{G^{1/n} - 1} \tag{5.3.4}$$

as shown in Figure 5.1, especially for n =10 (Hamamatsu R7056). We employed F $\sim$2 at the gain range of $10^4 \sim 10^6$ correponding to the operation voltages in the beam tests. By eq.(5.3.2) for LY =8.2 [p.e./MeV], a_{pe} $\sim$1 %. On the other hand, $\sqrt{a_{exp}^2 - a_{sim}^2}$ $\sim$3 % from the above results. It seems to be comparable in such a rough estimation.

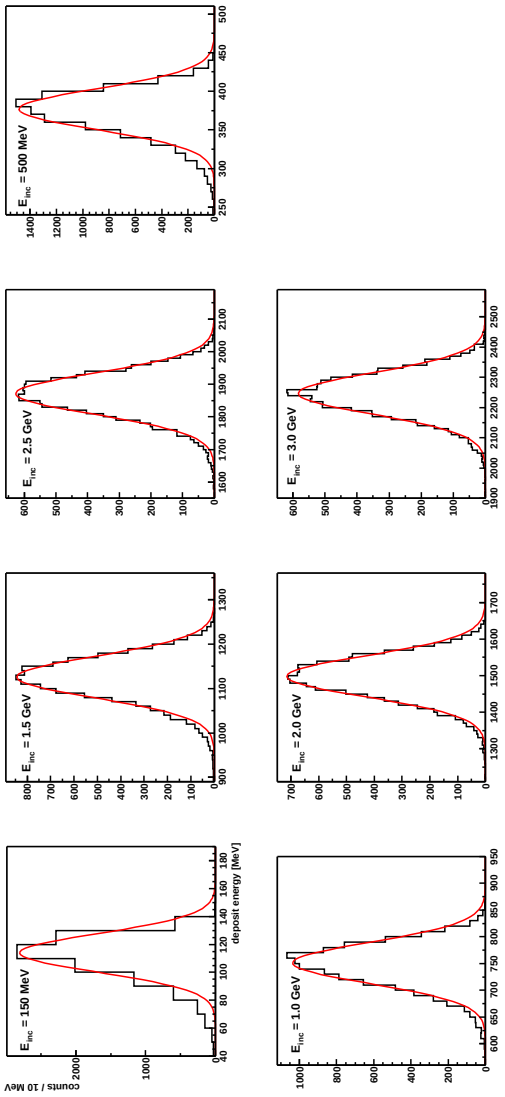

Figure 5.2: Deposit energy distribution for electrons with simulation

The electromagnetic shower initiated by electron incident on the single PWO crystals is simulated with the GEANT4 code. The crystal size is same as the our sample. The beam momentum is set to constant. The simulation is performed on the incident energy of 0.15, 0.50, 1.0, 1.5, 2.0, 2.5 and 3.0 [GeV], respectively. The spectrum are fitted with Gaussian at the full range.

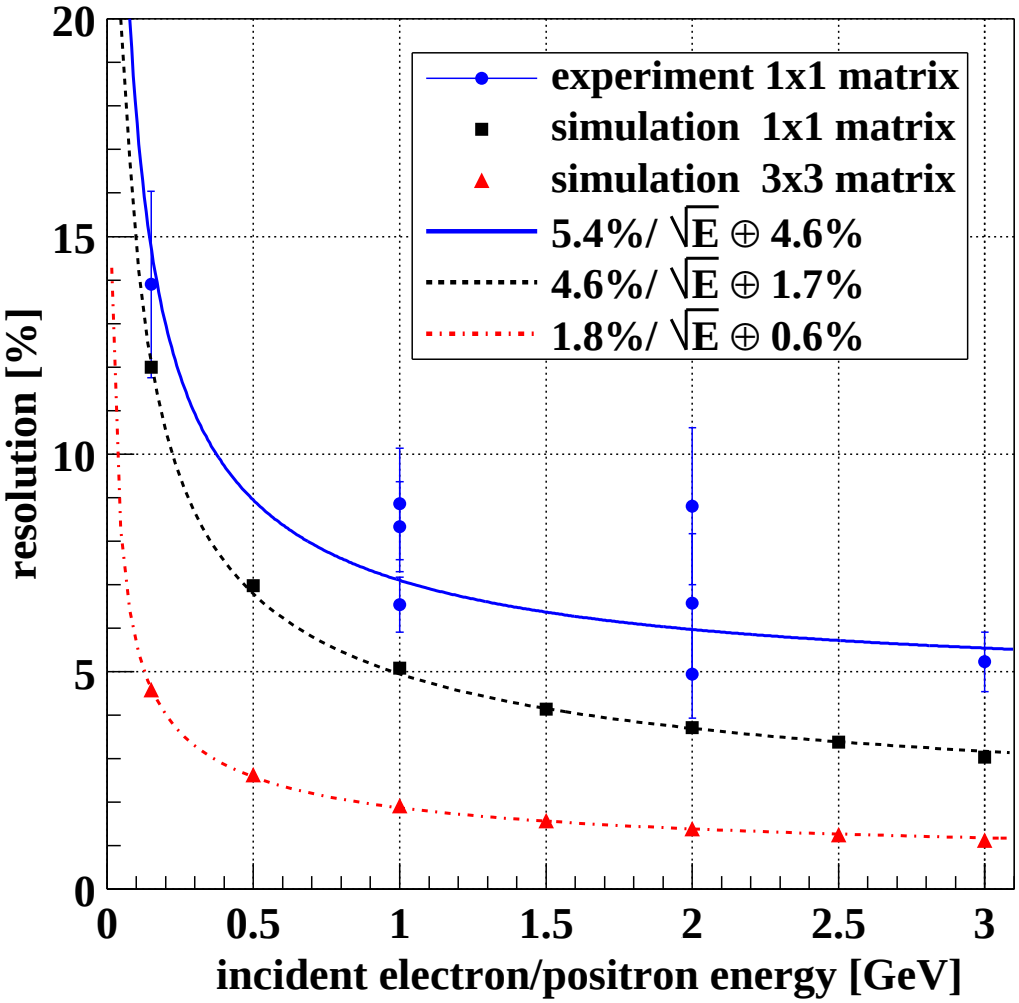

Figure 5.3: Energy resolution for the PWO crystal
The experiment data for the single PWO crystal is obtained from two beam tests at REFER and KEK-PS, the simulation data is calculated from the GEANT4 code for the single PWO crystal and nine crystals arranged in a 3× 3 matrix. The plotted data is fitted with eq.(2.3.1).

Chapter 6

Conclusion

We have concluded on this study that;

- The internal attenuation coefficient is 0.018[cm^{-1}] at the wavelength of 420 [nm].
- The PWO crystal is a small light output but very fast scintillator compared to the BGO crystal as shown in Table 6.1.
- There is the difference of the light yield with a factor of 2 between two PWO crystals manufactured in the same method.

Table 6.1: Measured scintillation properties

Samples	Light Yield [p.e./MeV]	Decay Time [ns]
PWO(A)	4.5	1.7 (30%), 5.6 (70%)
PWO(B)	8.2	1.2 (17%), 6.0 (83%)
BGO	404	185

- The average enegy containment in the single PWO crystal is 78 % of incident electron/positron energy.
- The energy resolution for the single PWO crystal is obtained to be

$$\frac{\sigma}{E} = \frac{5.6\%}{\sqrt{E}} \oplus 4.6\%$$

and consisted with the simulation results taken into account the photostatistics in the stochastic term, and will be improved to 1.8 $\%/\sqrt{E}$ with nine crystals arranged in a 3$\times$ 3 matrix.

Acknowledgements

We would like to thank Yoshie Furuhashi for her absolute collaboration and her carafully check to this manuscript, and Yuji Tsuchimoto for his invaluable help, and Toru Sugitate for his powerful comments. We are also grateful to Tomomi Ohgaki of VBL and Kiminori Goto of HiSOR for their technical supports in our beam test at REFER. We express our gratitude to all of T496 collaboration. This work was supported by High Energy Hadron Physics Laboratory of Hiroshima University[1].

[1] http://hiroh2.hepl.hiroshima-u.ac.jp

Bibliography

[1] The European Physical Journal

[2] P.Depasse et al., CMS Note 2000/009

[3] H.Shimizu et al., Nucl. Instr. and Meth. A447(2000)467

[4] R.Novotny et al., Nucl. Phys. B(Proc. Suppl.) 61B(1998)613

[5] M.Kobayashi et al., Nucl. Instr. and Meth. A447(2000)467

[6] S.Masuda et al., in Proceedings of the 25 Linear Acc elerator Meeting, July 12-24, (Himeji,Japan)2000.

[7] T.Ohgaki et al., Second Asian Particle Accelerator Conference, Sep 17-21, (Beijing, China) 2001, HUBP-07/01, physics/0109065.

[8] S. Giani et al., Geant4: An Object-Oriented toolkit for Simulation in HEP, CERN/LHCC 98-44, 1998.